An "Ultrasonic Image" of the Embryonic Universe

CMB Polarization Tests of the Inflationary Paradigm

1

An "Ultrasonic" Image of the Embryonic Universe: CMB Polarization Tests of the Inflationary Paradigm

1.1 Introduction

Why was there a Big Bang? Why is the universe not featureless and barren? Why are there fluctuations in the cosmic microwave background? In stark contrast to the convincingly answered "what" questions of cosmology (e.g. What is the age of the universe?, What is the geometry of the universe?), these "why" questions may instead evoke a sense of disillusionment. Is it possible that cosmology's "triumphs"—its answers to the "what" questions—are frustratingly inadequate, or worse, incomplete?

However, what if the "why" questions provide tantalizing hints of the ultimate origins of the universe? Then instead of crisis, we encounter an amazing opportunity—one that might provide answers to the most enigmatic question of all: How did the universe begin?

Inflation [1] is a daring paradigm with the promise to solve many of these mysteries. It has entered its third decade of successfully confronting observational evidence and emerged as cosmology's theoretical touchstone. Despite its many successes, inflation remains unproven. While skeptics must resort to increasingly finely tuned attacks [2, 3], inflation's proponents can only cite circumstantial evidence in its favor [4]. However, a conclusive detection of a primordial gravitational wave background (GWB) from inflation would be "the smoking gun" [5]. No other known cosmological mechanism mimics the GWB's imprint on the cosmic microwave background (CMB).

New technological innovations poise cosmology at the threshold of an exhilarating era—one in which future CMB data will winnow down the seemingly boundless "zoo" of cosmological models and test the hypothesis that an inflationary expansion of the universe took place in its first moments.

Inflation's unique imprint on CMB polarization has generated considerable attention from US science policy advisors [6, 7, 8, 9], who have all

enthusiastically recommended measuring CMB polarization. The reason for this excitement is clear: inflation explains a host of critical cosmological observations, and CMB polarization is the most promising, and perhaps only, way to glimpse the GWB.

This chapter describes how the Cosmic Gravitational Wave Background induces a specific type of CMB polarization and describes the first experiment dedicated to testing this most-promising signature of inflation. This experiment, the Background Imaging of Cosmic Extragalactic Polarization (BICEP) project, has recently embarked on its third observing season. We show preliminary data from the BICEP's first season obtained with a novel polarization modulation mechanism called the "Faraday Rotation Modulator". Our discussion ends with a description of exciting new technology with the potential to probe inflation down to the ultimate cosmological limit.

1.2 The inflationary universe

The CMB has historically been *the* tool to appraise inflationary cosmology. This is not surprising since the CMB is the earliest electromagnetic "snapshot" of the universe, a mere 380,000 years after the Big Bang. As such it probes the universe in a particularly pristine state—before gravitational and electromagnetic processing. Because gravity is the weakest of the four fundamental-forces, gravitational radiation (i.e. the GWB) probes much farther back: to $\simeq 10^{-38}$ seconds after the Big Bang ($10^6 t_{Pl}$ in Planck units). The GWB encodes the cosmological conditions prevailing at 10^{16} GeV energy scales. In contrast, the CMB encodes the physical conditions of the universe when radiation decoupled from matter at energy scales corresponding to 0.3 eV at $t \simeq 10^{56} t_{Pl}$. As experimentalists, we can exploit the primacy of the CMB by using the CMB's surface of last scattering as a "film" to "expose" the GWB—primordial reverberations in spacetime itself. Doing so will provide a "baby picture" of the infant universe; an "ultrasonic" image of the embryonic universe!

1.2.1 Quantum fluctuations in the inflationary universe

Inflation posits the existence of a new scalar field (the *inflaton*) and specifies an action-potential leading to equations of motion. Quantizing the inflaton field causes the production of perturbations (zero point fluctuations) [10]. While the inflaton's particle counterpart is unknown, its dynamics as a quantum field have dramatic observational ramifications [11]. All viable cosmological theories predict a spectrum of scalar (or energy density) per-

turbations that can then be tested against CMB temperature anisotropy measurements. Inflation predicts the spectrum of scalar perturbations, and additionally predicts tensor perturbations (i.e. the GWB). Inflation's unique prediction is the GWB, which is parameterized by the tensor-to-scalar ratio, r. An unambiguous detection of r will reveal both the epoch of inflation and its energy scale [5]. If, as theorists have speculated [12], inflation is related to Grand Unified Theories (GUT), then a detection of the GWB also will probe physics at energy scales one trillion times higher than particle accelerators such as the Large Hadron Collider [13].

Both energy density fluctuations (scalar perturbations) and gravitational radiation (tensor perturbations; the GWB) produce CMB polarization. The two types of perturbations are related in all inflation models, since both are generated by quantum fluctuations of the same scalar field, the inflaton [14]. The relationship between CMB polarization produced by scalars and tensors will provide a powerful consistency check on inflation when the GWB is detected. Similar relations, using recent detections of the *scalar* perturbation spectrum's departure from "scale invariance" [15] (primarily using CMB temperature anisotropy), have led to claims of "detection" of inflation, at least in the popular press [16]. Furthermore, NASA's Wilkinson Microwave Anisotropy Probe (WMAP) showed an anti-correlation between temperature and polarization at large angular scales, providing additional, albeit circumstantial, evidence in favor of inflation [17, 18].

The ultimate test of inflation requires a measurement of the tensor power spectrum itself, not only the predicted temperature-polarization correlation or the properties of the *scalar* power spectrum. Given a very modest set of external, non-inflation-specific parameters, including a simple cosmological chronology (specifying that inflation was followed by radiation domination, subsequently followed by matter domination), inflationary models can precisely predict the spatial correlations imprinted on the polarization of the CMB by the GWB, making it truly "the smoking gun."

1.2.2 The gravitational wave background: shaking up the CMB

Scalar metric-perturbations have no handedness, and are therefore said to be "parity invariant." While the GWB produces both temperature and polarization perturbations, the temperature perturbations are primarily associated with the change in potential energy induced by the gravitational waves, whereas the tensor-induced polarization perturbations are associated with spacetime stress and strain. The parity-violating polarization signature exists only if cosmological gravitational waves exist, as first demonstrated

by Polnarev [19]. As we will show, the amplitude of the polarization is determined by the energy scale of inflation, and its angular/spatial correlation structure is determined nearly exclusively by the expansion of the universe. While the energy scale (and, quite frankly, even *the existence*) of the inflaton is unknown, the post-inflation expansion history of the universe is *extremely* well understood. This is quite fortuitous for experimentalists hunting for the GWB as it dramatically restricts the range of our prey!

The separation between the inflationary and standard hot Big Bang dependencies is yet another manifestation of the interplay between inflation's quantum mechanical aspects and the Big Bang cosmology's classical dynamics. Although the inflationary perturbations are quantum mechanical in origin, they are small enough to be treated using linearized classical general relativity (the so-called WKB semi-classical approximation). So while the tensor-to-scalar ratio will probe quantum cosmology, the (classical) evolution of the scale factor allows for a precise prediction of the GWB's angular correlation imprint on CMB polarization. This separability, into a classical part (sensitive to the background evolution of spacetime) and a small, perturbative quantum component, makes the CMB's curl-mode polarization the most robust probe of inflation.

1.2.3 Observations and challenges

The inflationary model has revolutionized cosmology. Inflation solves the "horizon problem"—reconciling observations that show that regions of the universe have identical CMB temperatures (to a part in 10^5) by providing a causal mechanism for these regions to attain thermal equilibrium 380,000 years after the Big Bang. Inflation solves the horizon problem via an exponential, accelerating expansion of the universe at early times, prior to the "ordinary" Hubble-Friedmann expansion observed today. This rendered the entire observable universe in causal contact initially, and also accounts for the seemingly finely tuned spatial flatness of the universe observed by CMB temperature anisotropy experiments [20, 21, 22, 23, 24, 25].

Inflation also predicts a nearly scale-invariant spectrum of scalar perturbations. That *any* initial perturbations remain after the universe expanded by a factor of $\sim e^{60}$ is astonishing! Yet, surprisingly, the fluctuation level at the surface of last scattering arises naturally [14] in inflation as a consequence of parametric amplification, see Section 1.4.1. The residual fluctuations are observable in the CMB and indicate the epoch of inflation and the amount of expansion (the duration of inflation). This is inflation's solution to cosmology's "smoothness problem," accounting for the small, but non-vanishing,

level of perturbations. Regrettably, neither flatness nor smoothness are unique to inflation. Both have long histories, predating inflation. Flatness was anticipated on quasi-anthropic principles [26], and the universe's near-smoothness was predicted as the primordial matter power spectrum [27, 28, 29]. Recent CMB and galaxy cluster measurements [30, 31] have detected perturbations (possibly) resulting from phase-synchronized "quantum noise" (zero-point oscillations in the inflaton). These scalar, mass/energy perturbations, combined with the universe's spatial flatness, increase inflation's credibility since the e^{60}-fold expansion producing flatness *should* have also destroyed all initial perturbations. However, while there is abundant circumstantial evidence, there is one unique prediction of inflation: the primordial GWB, which produces an unmistakable imprint on the polarization of the CMB.

1.3 CMB polarization

The CMB is specified by three characteristics: its spectrum, the spatial distribution of its intensity (or temperature anisotropy), and the spatial distribution of its polarization. All three properties depend on fundamental cosmological parameters. Additionally, since CMB photons travel through evolving structures in the early universe on their way to our telescopes today, the CMB is also a probe of cosmic structures along the line of sight, which are, in some sense, "foregrounds"—either emitting, attenuating, or distorting the spatial and frequency power spectra of the background.

Originally proposed by Rees [32] as a consequence of an anisotropically expanding universe, the polarization of the CMB was unobserved for many decades. Although Rees' original model was found to be untenable, it was later corrected by Basko and Polnarev [33] in 1980. Nevertheless Rees' exploration attracted the attention of experimentalists [34, 35, 36] who initiated observations to measure CMB polarization. The polarization of the CMB, and its correlation with temperature anisotropy, was first detected by DASI [37]. The race to discover the wispy imprint of the GWB was on!

1.3.1 Temperature anisotropy produced by the GWB

When electrons in the primordial plasma prior to decoupling were irradiated with CMB photons, polarization of the microwave background was inevitable. Thomson scattering (low energy Compton scattering) produces polarization whenever photons from an anisotropic radiation field scatter off unbound electrons. Anisotropy in the CMB radiation field was pro-

duced by either mass/energy perturbations (over- and under-dense regions) or gravitational waves. When the photon field is decomposed into spherical harmonics, these two types of perturbation produce anisotropy of the quadrupolar variety ($Y_{\ell,m}$ with $\ell = 2$). There are five harmonics with $\ell = 2$, but only one of these, with $m = 0$, is azimuthally symmetric. The $Y_{2,m}$ with $m = \pm 2$ indicate that gravitational waves are spin-2 objects [38]. Gravitational waves "shear" spacetime and produce local violations of reflection, or parity, symmetry in the CMB polarization field [19, 33].

The GWB produces CMB temperature anisotropy as well. However, the temperature anisotropy is a scalar field on the celestial sphere and is dominated by the acoustic oscillations of radiation and matter, overwhelming the minute temperature anisotropy produced by gravitational waves. The temperature anisotropy induced by the GWB is also degenerate with other cosmological parameters [39, 40] and essentially undetectable at levels below the current WMAP3 limits, due to cosmic variance [41].

1.3.2 Polarization anisotropy produced by the GWB

Fortunately, however, the CMB polarization's *tensorial nature* breaks the parameter degeneracy. Using an analog of Helmholtz's vector calculus theorem valid for spin-2 fields on the celestial sphere, CMB polarization maps, like Figure 1.1, can be decomposed into two scalar fields or "modes" [39, 40]. The advantage of manipulating two scalar fields, as opposed to one tensor field, is self-evident.

One of the scalar fields is, essentially, the gradient of a scalar-potential and is known as "E-mode," or "gradient-mode," polarization by analogy to the electric field. The E-mode polarization is invariant under parity transformations. The second component, called "B-mode," or "curl-mode," polarization is analogous to the the curl of a vector-potential. If inflation produced a sufficient amount of gravitational radiation, then future maps of CMB polarization will be admixtures of both modes (though the E-mode polarization will dominate by *at least* a factor of ten). For reference, simple one-dimensional maps of pure E- and B-modes are shown in Figure 1.2. Appraising the behavior of the circular maps with respect to reflections across the map's diameter reveals the symmetry of the underlying polarization mode.

The pioneering work by Polnarev [19] was the first to identify a unique observational signature of gravitational waves; one that would *only* be manifest in the polarization of the CMB. Polnarev's key insight was to recognize that asymmetric shear induced by gravitational waves would induce a polar-
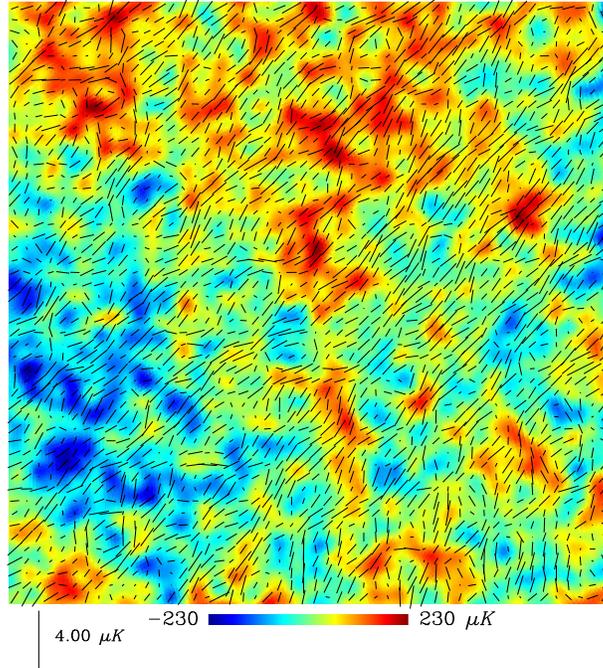
Fig. 1.1. A simulated noiseless map of CMB polarization and temperature anisotropy. The simulation represents an $18° \times 18°$ map of the CMB's temperature, E-mode, and B-mode polarization. The temperature (gray scale) and E-mode polarization reveal the classical cosmological parameters such as the mass density, geometric curvature, and composition of the universe (i.e. "dark" versus ordinary matter). The B-mode, or "curl," polarization is *only* generated by primordial gravitational waves and is indicated by regions where reflection symmetry is locally violated. The vertical scale bar at the lower left indicates polarization at the 4 μK level. The polarization vectors are the sum of E- and B-mode polarization, but are dominated by E-mode polarization (B-mode polarization is less than $0.1\,\mu$K in this simulation, corresponding to a tensor-to-scalar ratio $r \sim 0.1$). Figure credit: Nathan Miller.

ization pattern significantly different from that produced by scalar perturbations, such as those shown in the right-hand side of Figure 1.2. Polnarev predicted that gravitational waves would be the only plausible source of parity violation on a cosmological scale. In the more modern language of E- and B-modes, this is equivalent to predicting the existence of B-modes imprinted on the CMB by a primordial GWB.
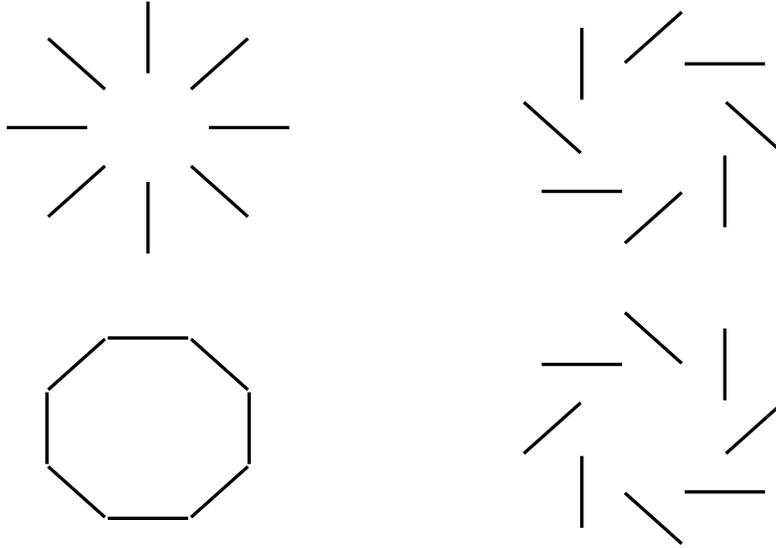
Fig. 1.2. Parity symmetric E-mode (or "gradient-mode") polarization patterns (left side), and B-mode (or "curl-mode") patterns (right side) in real space. Figure credit: Nathan Miller.

1.4 The origin of the gravitational wave background

How can *any* perturbations originating from quantum fluctuations in the primordial inflaton field survive the explosive expansion by a factor of e^{60}? After all, a hallmark of inflation is that this expansion dilutes the curvature of the universe from any primordial value to precisely flat. In fact, since the GWB is a radiation background exactly like the CMB, the subsequent expansion following inflation dilutes the GWB's energy density by a factor of a^4, where a is the cosmic scale factor. Since the GWB energy density today is at least one billion times smaller than the CMB's energy density, this means that it was utterly insignificant for all times, including at decoupling.

This brings us to another potentially troubling "why" question: Why are gravitational waves expected to persist to last-scattering, and leave a detectable imprint on the CMB, if the very cosmological model predicting them produces an expansion that should render them negligible? A hint at the answer to this question comes from a rather unlikely source: a playground swingset!

1.4.1 Parametric resonance and amplification

Parametric amplification is exemplified by an undamped pendulum of length L whose suspension point, y, is driven vertically $y = A \cos 2\pi f t$. To highlight the connection between (1) the GWB, (2) the vertically driven pendulum, and (3) the laser, we term the periodic driving force the "pump." Pump energy at frequency f drives the pendulum into resonance and can even amplify small random thermal vibrations of an (initially stationary) pendulum into oscillation.

For simplicity, the angle between the pendulum and the vertical, ϕ, is taken to be small, and the equation of motion for ϕ becomes:

$$\ddot{\phi} + (\omega_0^2 + \Omega^2 \cos 2\pi f t)\phi = 0 \tag{1.1}$$

where $\Omega^2 = (2\pi f)^2 A/L$.

Equation 1.1 is known as *Mathieu's equation.* In Mathieu's equation, ω_0 is the natural frequency of the pendulum, and the *parameter* Ω determines the resonant behavior of the pendulum, leading to *parametric resonance.* While the equations of motion are linear with respect to ϕ, the effect of the pump is not additive (as it would be if the suspension point were to be horizontally modulated), but rather *multiplicative.*

To find periodic solutions to Equation 1.1, we construct the following *ansatz*:

$$\phi = \varphi_+ e^{+i\pi f t} + \varphi_- e^{-i\pi f t} \tag{1.2}$$

In general, both stable and unstable solutions of Equation 1.1 can be obtained. So called "resonance bands" are separated by regions of stability where the amplitude of ϕ is constant. Unstable solutions exponentially diverge (as $\phi \simeq e^t$). Both types of solutions will be important in the context of gravitational waves. Solving Equation 1.1 using Equation 1.2 leads to

$$[\omega_o^2 - (\pi^2 f^2)]\varphi_\pm + \frac{\Omega^2}{2}\varphi_\mp = 0 \tag{1.3}$$

where third-harmonic generation effects have been ignored. Stable solutions to the (two) Equations 1.3 are non-trivial and solvable for $\varphi_\pm$ when the following self-consistency relation holds between the pump amplitude, frequency, and natural frequency of the pendulum:

$$\Omega^2 = 2[\omega_o^2 - \pi^2 f^2] \tag{1.4}$$

The first, or *fundamental*, resonance condition for the pump frequency

is $f = \omega_0/\pi$, which implies that pumping at *twice* the pendulum's natural frequency defines the boundary of incipient instability even if the pump amplitude is small ($|\phi(t)| \neq 0$ even as $\Omega, A \to 0$).

The pumping strategy mentioned above shares similar features with a similar application on the playground. Assisted swinging on a swingset is a resonant system with pump-power supplied by two assistants, one at each of the two displacement maxima; that is, with pump frequency $f = 2\frac{\omega_0}{2\pi}$. When this condition holds, $\Omega = 0$ and only small amounts of pump energy are required to maintain the swing's oscillatory behavior, even in the presence of significant frictional damping (which has been ignored here).

In fact, while less social (and more dangerous) than assisted pumping (using two friends), vertical pumping employing parametric resonance allows the rider to initiate resonance by themselves (by raising and lowering their center of mass—alternately standing and squatting on the swing). Surprisingly, the amplification of small initial perturbations via parametric resonance provides a fruitful analogy for the theory of gravitational wave amplification.

1.4.2 Parametric amplification of the GWB

Gravitational waves have unique and fascinating cosmological properties. While the contribution of these waves to the energy density of the universe today is minuscule, parametric amplification of these primordial quantum fluctuations of the inflaton field causes the waves to grow large enough to become potentially observable. If the imprint of these primordial perturbations is observable, an understanding of the parametric amplification process allows us to optimize our observational requirements—regardless of the magnitude of the inflationary GWB.

In our simplified cosmology, spacetime is smooth and flat. On top of this background a tensor field, representing the GWB, is suffused. The metric of this spacetime is obtained by solving the Einstein equations

$$G_{\alpha\beta} = 8\pi G T_{\alpha\beta}$$

where G is Newton's constant of universal gravitation. For empty space the stress-energy tensor $T_{\alpha\beta} = 0$, leading to

$$ds^2 = a(\eta)^2[d\eta^2 - (\delta_{\alpha\beta} + h_{\alpha\beta})dx^\alpha dx^\beta] \qquad (1.5)$$

where $\delta_{\alpha\beta}$ is the Kronecker delta function, and η, the *conformal time*, is related to the (time-dependent) cosmological scale factor a via $d\eta = dt/a$.

The (linearized) perturbation tensor is both transverse-symmetric ($h_{\alpha\beta} = h_{\beta\alpha}$) and traceless ($\sum_{\alpha} h_{\alpha\alpha} = 0$). We seek solutions, which are separable into a tensorial part and a scalar part, of the following form

$$h_{\alpha\beta} \equiv \sqrt{8\pi G}\,\frac{\nu}{a}\,\epsilon_{\alpha\beta}\,e^{ik\eta} \tag{1.6}$$

where $\epsilon_{\alpha\beta}$ is the gravitational wave polarization tensor. The rank-two tensors $h_{\alpha\beta}$ and $\epsilon_{\alpha\beta}$ are transverse and traceless, leading to two independent polarization modes denoted "+" and "×." Solving Einstein's equations yields wave equations for ν, the (scalar) amplitude of the set of equations $h_{\alpha\beta}$

$$\begin{aligned}
\ddot{\nu} + (k^2 - \ddot{a}/a)\nu &= 0 \\
\ddot{\nu} + (k^2 - U_{eff})\nu &= 0
\end{aligned} \tag{1.7}$$

Here, overdots denote derivatives with respect to conformal time (e.g. $\dot{x} = a\frac{dx}{dt}$), and in the second equation we have replaced $U_{eff} = \frac{\ddot{a}}{a}$, which acts as a time-dependent *effective potential* [42]. We recognize Equation 1.7 as a version of Mathieu's equation for the vertically driven pendulum, Equation 1.1, once the following substitution is made in Equation 1.1:

$$-\Omega^2 \cos 2\pi f t \equiv U_{eff}(a)$$

In contrast to the vertically driven pendulum, variation of the pump parameter U_{eff} does not lead to runaway growth. Rather, the time-varying effective potential amplifies long-wavelength oscillations relative to short wavelength oscillations.

For an isotropic, homogenous universe consisting of a fluid with pressure p and density ρ we can express

$$\begin{aligned}
U_{eff}(a) &= \frac{d}{dt}\left(a\frac{da}{dt}\right) \\
&= \left(\frac{da}{dt}\right)^2 + a\frac{d^2a}{dt^2} = a^2 H^2 + a\frac{d^2a}{dt^2} \\
&= a^2\left[\frac{8\pi G\rho}{3} - \frac{4\pi G}{3}(\rho + 3p/c^2)\right]
\end{aligned} \tag{1.8}$$

Here, we have employed the definition of the Hubble parameter $H(a) \equiv \frac{1}{a}\frac{da}{dt} = \sqrt{8\pi G\rho(a)/3}$. For convenience, the equation-of-state relating pressure, p, and density, ρ, is taken as $p = \gamma\rho c^2$ (where γ is a scalar that depends on the cosmological epoch under consideration). As the universe expands,

it dilutes: $\rho = \rho_*(\frac{a}{a_*})^{-3(1+\gamma)}$. This equation is valid at any epoch, or correspondingly, for any value of a. When we consider a *specific* epoch we label it a_*. From Equation 1.8 we obtain

$$U_{eff}(a) = \frac{8\pi G \rho a^2}{3}\left[1 - \frac{(1+3\gamma)}{2}\right] = \frac{4\pi G \rho_*(1 - 3\gamma)a_*^2}{3}\left(\frac{a}{a_*}\right)^{2-3(1+\gamma)}$$

which can be written as

$$U_{eff}(a) = \frac{4\pi G \rho_*(1 - 3\gamma)a_*^2}{3}\left(\frac{a}{a_*}\right)^{-(1+3\gamma)} \tag{1.9}$$

The evolution of the effective potential depends crucially on the cosmological epoch, via the relationship between density and pressure. For example, during radiation domination, $\gamma = 1/3$ and the effective potential $U_{eff}(a) = 0$. Recalling Equation 1.7, when either $U_{eff}(a) = 0$ or $k^2 \gg U_{eff}$, the solutions for ν, the gravitational wave amplitude, are simple plane-waves. These purely oscillatory solutions prevail *whenever $k \gg U_{eff}$*, but especially during radiation domination when the dilution of the GWB is identical to that of *any* radiation background, such as the CMB.

For future reference, using the definition of the Hubble parameter $H(a)$ in terms of density $\rho(a)$, we can write

$$U_{eff} = \frac{(1 - 3\gamma)k_*^2}{2}\left(\frac{a}{a_*}\right)^{-(1+3\gamma)} \tag{1.10}$$

where $k_* \equiv a_* H(a_*)$.

Using Equations 1.6 and 1.9, we can solve Equation 1.7 for the gravitational wave amplitude

$$h = \sqrt{8\pi G}\,\frac{a_*}{a}e^{[ik(\eta - \eta_*)]} \tag{1.11}$$

Gravitational waves "enter" the horizon when $k \simeq 1/\eta$, and as the universe Hubble-expands, they are damped by the adiabatic factor $1/a$, just like radiation. Example solutions of Equation 1.11 are shown in Figure 1.3.

1.4.3 The effective potential

We have shown that the equation-of-state parameter γ determines the effective potential, subsequently determining the evolution of the GWB, at least during radiation domination. In this subsection we examine solutions in the other important cosmological epochs. We will see that specifying γ versus
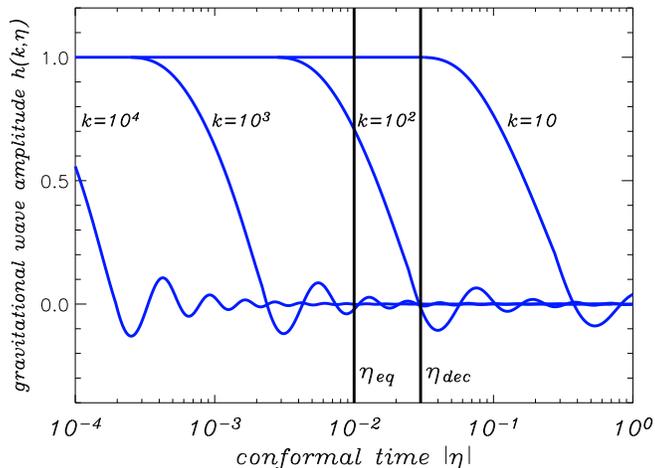
Fig. 1.3. Gravitational wave amplitude as a function of conformal time for four different wavenumbers. Gravitational waves are constant, and equal in amplitude independent of wavelength, before entering the horizon when $k\eta \sim 1$, leading to decay. Equivalently, waves with $k \ll U_{eff}(a)$ (long wavelength waves) experience the effective potential, forestalling their decay. Short wavelength waves never interact with the potential, continuously decaying adiabatically instead. Long wavelength modes essentially "tunnel" through the barrier with no diminution of their amplitude until after radiation-matter equality. Figure credit: Nathan Miller.

cosmological scale not only allows us to predict the advantages of indirect detection of the GWB (using B-modes) over direct detection methods, but also to *optimize* experimental CMB polarization surveys themselves.

In the following, the subscripts "-" and "+" will denote quantities before and after inflation ends, respectively. If a_{end} denotes the scale factor *at* the end of inflation, this means that for $a < a_{end}, \gamma < -\frac{1}{3}$. After inflation ends $a > a_{end}$ and $\gamma_+ > -\frac{1}{3}$. For example, $\gamma_+ = 1/3$ corresponds to the equation-of-state for radiation; that is, when inflation ends the universe is radiation dominated.

More generally we can say that at the moment when $a = a_{end}$, accelerated expansion $(d^2a/dt^2 > 0)$ changes to decelerating expansion $(d^2a/dt^2 < 0)$, and during inflation the cosmological horizon *decreases* [14]. Hence, from Equation 1.10, for $a < a_{end}$,

$$U_{eff} = \frac{(1 - 3\gamma_-)k_*^2}{2}\left(\frac{a}{a_*}\right)^{|1+3\gamma_-|} \tag{1.12}$$

which increases with a, and when $a > a_{end}$

$$U_{eff} = \frac{(1 - 3\gamma_+)k_*^2}{2}\left(\frac{a}{a_*}\right)^{-|1+3\gamma_+|} \tag{1.13}$$

which decreases with a. Since the transition from γ_- to γ_+ occurs quasi-instantaneously, the effective potential is discontinuous; $\gamma_+ > \gamma_-$. For more accurate results we should properly treat the reheating phase, when the inflaton is converted into particles and radiation. Interestingly, parametric resonance techniques can also be used to describe reheating [43].

Now it should be clear why $\frac{\ddot{a}}{a}$ was called an *effective potential*. Since U_{eff} is maximized when inflation ends, there are two epochs, $a_- < a_{end}$ and $a_+ = a_{end}$, where $k^2 = U_{eff} < U_{max}$. Thus there are two wavelength regimes that determine the form of solutions to Equation 1.7. High-frequency waves with $k/k_H \gg \eta_{eq}$ enter the horizon well before matter-radiation equality, then decay as the universe expands as in Equation 1.11 [44, 45].

Long wavelength waves, on the other hand, satisfy

$$\ddot{\nu} - U_{eff}(a)\nu = 0 \tag{1.14}$$

To solve Equation 1.14 we must first determine the behavior of the effective potential in a form that is valid during any cosmological epoch.

1.4.4 Timing is everything: the cosmic chronology

To analyze the impact of the effective potential on long wavelength gravitational waves we must solve for $U_{eff} \sim \ddot{a}/a$, recalling that the derivatives are with respect to conformal time, η. We therefore require the relationship between the scale factor and conformal time. For reference, we recall that during radiation domination $U_{eff} = 0$ for all wavelengths.

1.4.4.1 Evolution of the effective potential

During the epoch of matter domination, it is convenient to parameterize the evolution of the scale factor versus time as $a \sim t^\alpha$ with $\alpha = 2/3$. Using the definition of conformal time, we have $d\eta = dt/a$, implying that $a = \eta^{\frac{\alpha}{1-\alpha}}$ or $a(\eta) = \eta^2$ during matter domination. Using this, we find that the effective potential during matter domination *decays* as $U_{eff}(a) \propto 1/a$, as described quantitatively in Equation 1.13 and displayed in Figure 1.4.

Finally we must calculate the effective potential during inflation, when the scale factor grows as $a = e^{Ht}$, implying $d\eta = e^{-Ht}dt$. Integrating, we find $\eta = (1 - e^{-Ht})/H$ or that
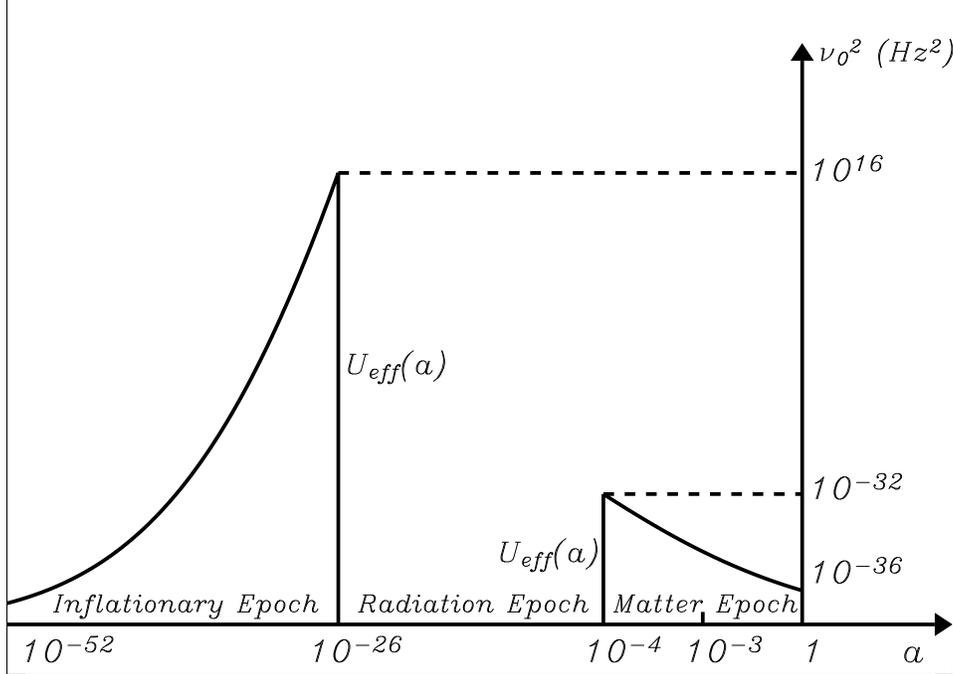
$$a \simeq \frac{1}{H|\eta|} \tag{1.15}$$

Fig. 1.4. The parametric amplification of primordial gravitational waves is governed by the evolution of the effective potential as a function of cosmic scale factor, a. This figure, adapted from [42], shows the effective potential in three important cosmological epochs. Here the wave's frequency ($\nu_0 = ck$) is expressed in present-day units, when $a = 1$. Long wavelength waves ($k^2 < U_{eff}$) "tunnel" through the potential and remain constant until inflation ends. Short wavelength waves never experience the potential and instead decay adiabatically (as $1/a$). During radiation domination, the effective potential vanishes and all waves inside the horizon decay. Finally, any waves that survive until matter-radiation equality imprint the CMB sky prior decoupling. Therefore, these waves are comparable to, or larger than, the horizon at decoupling, subtending an angle of $\simeq 2°$ on the sky today. Figure credit: Nathan Miller.

during inflation, leading to

$$U_{eff}(a) = 2H^2a^2 \tag{1.16}$$

That is, the effective potential *grows* quadratically.

1.4.4.2 Evolution of the GWB

With the effective potential expressed in terms of conformal time we can easily solve the gravitational wave equation. During *inflation*, $a \sim 1/\eta$ so $U_{eff} \propto 2/\eta^2$ (as anticipated from Equation 1.12). For long wavelength waves, the parametric equation is

$$\ddot{\nu} - \frac{2}{\eta^2}\nu = 0 \qquad (1.17)$$

Solutions to Equation 1.17 are easily verified to be $\nu \sim 1/\eta$, or $\nu(a) \sim a$. Since $h(a) \equiv \sqrt{8\pi G}\nu/a$ (Equation 1.6) we see that the gravitational wave amplitude during the inflationary epoch is constant for waves with wavelengths smaller than $U_{eff}(a < a_{end})$, or equivalently

$$h(k, \eta) = \frac{\sqrt{8\pi G}}{\eta a} \qquad (1.18)$$

During *radiation domination*, $U_{eff} = 0$ and the gravitational waves are oscillatory functions that redshift and dilute adiabatically as

$$h = h_- \frac{a_-}{a} e^{[ik(\eta - \eta_-)]}$$

During *matter domination*, although the effective potential has the same dependence on η as it does during inflation, the scale factor depends on conformal time in a different way. This leads to a *different* gravitational wave solution. During matter domination, $\eta = \sqrt{a}$ and so $h = \nu/a \sim 1/a^{3/2}$, implying that gravitational waves decay even when their wavelengths are long ($k < U_{eff}(a_{eq})$). Once again, however, longer wavelengths are preferentially preserved relative to short wavelength modes.

Thus we have the following cosmic chronology. During inflation, long wavelength gravitational waves are "frozen" outside the horizon, or equivalently, are spared from adiabatic decay as they tunnel through the effective potential, which grows quadratically as the universe inflates. At the beginning of radiation domination (end of inflation; a_{end}), the effective potential drops to zero. All waves that are within the horizon decay adiabatically. The largest waves persist until decoupling, when the universe is matter dominated and the potential again becomes critically important. The primordial scale-invariant distribution of waves is transformed twice; first during inflation, and later during matter domination. In both cases, longer wavelength perturbations are overpopulated with respect to their short wavelength counterparts.

1.4.5 Quantum gravitational wave effects

We can make an analogy between the GWB and the laser here by rewriting the GWB parametric equation (Equation 1.7) as $\ddot{\nu} + (k^2 - U_{eff}(a))\nu =$

$\ddot{\nu} + k_{eff}^2 \nu = 0$. For $k_{eff}^2 > 0$ the solutions are constant oscillatory functions, while for $k_{eff}^2 < 0$ we have decaying solutions. Similar derivations [44, 45], using creation and annihilation operators, are particularly useful for exploring the connections between the quantum properties of the GWB and the laser (which can also be derived using creation and annihilation operators). This derivation is possible because the gravitational waves, or gravitons, are bosons, as are the laser's photons. In both cases, the pump need not be periodic.

However, the analogy cannot be taken much further. For the prototypical three-level laser, coherent amplification is obtained via stimulated emission from a metastable state. The metastable state's occupation number is inverted with respect to the ground state. For the GWB there is no such population inversion, nor stimulated emission, and thus the GWB is an incoherent, stochastic radiation background, not unlike the CMB.

We are interested not only in the properties of a *single* gravitational wave, but also in the behavior of a stochastic ensemble of waves, tracing its origin to "quantum noise" in the inflaton. To quantify the preferential population of long wavelength gravitational waves, we calculate the initial number of gravitons, or occupation number, for given conformal wave number k when $a \ll a_{end}$, denoted as N_{in}. We construct the correlation function of this stochastic background by considering the energy of a collection of N oscillators, each with energy $E = \hbar\omega(n + \frac{1}{2})$ in state n. Using terminology familiar from laser physics, the number of gravitons [46] in a volume $V(a)$ is the (renormalized) energy divided by the product of the frequency and the reduced Planck constant, $\hbar$:

$$N_{in} = \frac{c^4 V(a)}{32 G \pi \hbar \omega(a)} \Big\langle \Big(\frac{dh_\alpha^\beta}{dt}\Big)\Big(\frac{dh_\beta^{\alpha*}}{dt}\Big)\Big\rangle \tag{1.19}$$

In Equation 1.19, $*$ indicates complex conjugation, the angled brackets $\langle \ldots \rangle$ denote averages over polarization, propagation angles, time, and volume. The average results in a constant factor that is subsequently incorporated along with the physical constants into a constant κ. Finally, we define $\omega \equiv k/a$, thus simplifying the time derivatives: $\frac{dh_\beta^\alpha}{dt} = \omega h_\beta^\alpha$ and $V(a) = V_0 a^3$.

As result we have

$$N_{in} \approx \kappa \Big(\frac{h_- a_-}{a}\Big)^2 \Big(\frac{k}{a}\Big)^2 \Big(\frac{k}{a}\Big)^{-1} V_0 a^3 \tag{1.20}$$

$$\approx \kappa h_-^2 a_-^2 k V_0 \tag{1.21}$$

which does not depend on a. Similarly, the *final* mode occupation number at the end of inflation, N_{out}, when $a \gg a_{end}$ and $k^2 \gg U_{eff}$ is

$$N_{out} \approx \kappa h_+^2 a_+^2 k V_0$$

which is also independent of time and a. For $a_- < a < a_+$, when $k \ll U_{eff}$ (long wavelength gravitational waves), the solution for the gravitational wave amplitude is $\nu \approx a$. For a scale invariant spectrum h is constant, meaning that gravitons are created with the same amplitude ($h_- \approx h_+$). This leads to the amplification factor:

$$A = \frac{N_{out}}{N_{in}} \approx \left(\frac{a_+}{a_-}\right)^2 \tag{1.22}$$

which is larger than unity if $k^2 < U_{max}$. Therefore, long wavelength gravitational waves are amplified with respect to their short wavelength counterparts (which experience the potential for a much shorter time). This is evident from Figure 1.4. Intermediate wavelength waves ($k^2 \sim U_{max}$) do not experience the effective potential until much later than their long wavelength counterparts, and very short wavelength waves, with $k^2 > U_{max}$, do not enter the potential at all.

As such, if all waves start with the same initial amplitude (Harrison-Zeldovich spectrum), short wavelength waves will decay by a quadratic factor relative to longer waves. We note that the change in scale factor during inflation can be enormous; expansion by factors of 10^{30} are common for models that produce sufficient inflation to make spacetime flat. In the context of the GWB, only the *difference* in the expansion of the universe between the horizon-entry time for short wavelength modes compared to that for long wavelength modes is relevant.

1.5 Observational consequences

To illustrate the significance of parametric resonance, it is useful to consider the following generic inflation scenario where the equation-of-state parameter changes from $\gamma_- = -1$ to $\gamma_+ = 1/3$; that is, radiation domination immediately follows inflation. Using Equation 1.10, in such a scenario a wave with $k_{end} \simeq a_{end} H_{end}$ enters the effective potential just as inflation ends. As such it is not amplified. A long wavelength wave enters the potential earlier when $a_- \simeq H/k$. We are free to define the scale factor at the end of inflation as $a_{end} = 1$. Thus from Equation 1.22, with $a_+ = a_{end} = 1$, the

amplification scales with wavevector as $A \sim \left(\frac{H^2}{k^2}\right)$, assuming H is constant during inflation. The implication of this equation is clear: if the primordial gravitational wave spectrum is scale invariant ($h_- \simeq h_+$), then post-inflation it is transformed into a strongly wavelength-dependent spectrum.

Not all of these amplified waves survive to imprint the CMB with B-mode polarization. Waves that are larger than the present-day horizon are frozen and are not amplified. Additionally, all sub-horizon waves decay by the adiabatic factor $\frac{a_{rad}}{a_{eq}}$ from the onset of radiation domination at reheating to the epoch of matter-radiation equality.

1.5.1 Tensor power spectrum: amplitude and angular structure

More generally, we are interested in the variance of $h(k, \eta)$ as a function of wave number, also called the *tensor power spectrum*, defined as

$$P_t(k) \equiv \frac{|h(k, \eta)|^2}{k^3}$$

From Equation 1.18 we recall that $h(k, \eta) = \frac{\sqrt{8\pi G}}{\eta a}$. Since $\eta \simeq 1/aH$ (Equation 1.15), we find

$$P_t(k) = \frac{8\pi G H^2}{k^3} \tag{1.23}$$

Thus, measuring the tensor power spectrum probes the Hubble constant during inflation and is proportional to the energy density of the inflaton (since $H^2 \propto \rho$). The amplitude of the tensor power spectrum is directly revealed by the amplitude of the CMB curl-mode polarization power spectrum. If inflation occurs at energy scales comparable to E_{GUT}, CMB B-mode polarization allows us to test physics at scales one trillion times higher than the highest energy produced in terrestrial particle accelerators!

We have shown how the tensor power spectrum's amplitude depends on the energy scale of inflation. Now our aim is to qualitatively determine the angular correlation properties, or shape, of the tensor power spectrum $P_t(k)$. Doing so allows us to optimize observations of the GWB, for as we will see, $P_t(k)$ has a well-defined maximum as a function of wavenumber, or equivalently, angle subtended on the sky.

In the context of the driven undamped pendulum, the *ansatz* solutions, Equation 1.2, can grow exponentially or remain constant. The *long* wavelength gravitational waves amplitudes are also stable when they are larger than the cosmological horizon. Short wavelength gravitational waves decay adiabatically because they are always within the horizon during inflation. In

the context of parametric amplification, long wavelength waves ($k^2 < U_{eff}$) are said to be "super-horizon" or non-adiabatic.

Since the extremely high-frequency waves are always above the potential barrier, they continuously decay and leave no observable signature. The longest waves enter the horizon near decoupling when the effective potential is decaying. Waves that experience the matter-dominated effective potential close to decoupling are amplified the most, leading to a well-defined peak in the tensor power spectrum on scales comparable to the horizon at decoupling. This scale subtends an angle of $\simeq 1°$ to $2°$ on the CMB sky today, and therefore this is the characteristic scale of the tensor and B-mode angular correlation function.

1.5.2 Direct versus indirect detection of the primordial GWB

It is perhaps instructive to ask whether the primordial GWB could be directly detected *today*. While scalar, or mass-energy, perturbations are amplified by gravitational condensation, the tensor GWB is not. Directly detecting the GWB *today* (redshift $z = 0$) by, for example, LIGO, would be extremely difficult since, like the primordial photon background (the CMB), the energy density of the primordial GWB dilutes (redshifts) by the fourth power of the scale factor as the universe expands. However, the GWB imprints curl-mode polarization on the CMB at the surface of last scattering (at $z \sim 1,100$ or 380,000 years after the Big Bang). Therefore, the energy density of the GWB at last scattering was more than *one trillion times* ($1,100^4$) larger than it is now.

Ultimately, direct detection experiments such as ESA's *LISA*, NASA's *Big Bang Observer*, or Japan's *DECIGO* experiment will provide further tests of the inflationary model, such as measuring the GWB power spectrum at wavelengths approximately twenty orders of magnitude smaller than those probed by CMB polarization [47, 48, 49]. As we have seen, the current spectral density of these short wavelength waves is extremely small, and these experiments are fraught with contamination from "local" (i.e. non-cosmological) sources. However, given a detection of the primordial GWB at the surface of last scattering using CMB polarization, these direct detection campaigns will measure the fine details of the inflaton potential, making them at least well justified, if not mandated.

1.5.3 Indirect detection of the GWB: optimizing CMB polarization observations

Parametric amplification had important ramifications for the design of the first experiment dedicated to measuring the GWB—BICEP (Background Imaging of Cosmic Extragalactic Polarization). While the amplitude of the GWB is unknown, parametric amplification allows the structure of the B-mode's angular correlation function to be accurately calculated given only modest assumptions about the cosmic equation-of-state and evolution of the scale factor. This allowed the BICEP team to optimize the angular resolution of our search for the B-mode signature; motivating both BICEP's optical design as well as its survey design (required sky coverage).

BICEP probes the inflationary GWB primarily at large angular scales corresponding to the largest wavelength waves that entered the horizon near decoupling ($\simeq 2°$). Since the tensor angular correlation function peaks on these scales, to obtain statistical confidence in our measurement it is only necessary for BICEP to probe a small fraction of the sky ($\simeq 3\%$), rather than diluting our observing time over the entire sky. This allows us to target the cleanest regions of the sky—those with minimal contamination from galactic dust or synchrotron radiation, both of which are known to be polarized.

1.5.4 Detectability of the CMB B-mode polarization

Nearly thirty years passed between the discovery [50] of the CMB by Robert Wilson and Arno Penzias (Charles Townes' Ph.D. student) and the first detection of temperature anisotropy [51] by COBE at the ten parts-per-million level. If inflation occurred at the GUT-scale, it would produce curl-mode polarization at the ten parts-per-*billion* level.

Thanks to the innovative technologies produced by our collaboration, detection of this signal is conceivable. BICEP—the ground-based polarimeter we built—will achieve higher sensitivity to the GWB than either NASA's WMAP (Wilkinson Microwave Anisotropy Probe) or the Planck satellite.

BICEP is both a pioneering experiment and a long-range, two-phase campaign designed to mine the CMB sky using innovative technology. BICEP is an attempt to probe even farther back than the last scattering surface: to the very beginning of the universe, the inflationary epoch. Detecting the GWB requires ultrasensitive technology, only recently invented. An understanding of parametric amplification allows us to precisely estimate the spatial power spectrum imprinted on the CMB's polarization by the primordial GWB. This leads to a very general optimization of experimental campaigns [52]. To detect the GWB's polarization imprint, only modest an-

gular resolution is required—corresponding to a small refractor. This small refractor can probe the inflationary B-mode polarization nearly as well as a reflecting telescope twenty-times larger in diameter!

As shown in the following section, BICEP's small size has several important ancillary benefits—most notably that its smaller aperture results in a much higher-fidelity optical system, one with no obscuration or secondary mirror to induce spurious polarization. Additionally, the refractor is easy to shield from stray light—which is particularly important when probing signals one billion times smaller than the background.

1.6 Experimental quantum cosmology: the BICEP project

BICEP [53, 54] is a bold first step toward revealing the GWB. Ultimately, only a small telescope like BICEP can be cooled entirely to nearly the temperature of the CMB itself—a condition not previously achieved, even in space. BICEP's elegant design (see Figure 1.5) has proven extremely attractive for proposed future experiments [55, 56], which have receiver concepts closely resembling BICEP.

BICEP is the first experiment to directly probe for the primordial GWB. Even Planck, when it is launched in 2008, will not be as sensitive to the GWB signal as BICEP (which will already have completed first-phase observations). A comparison of BICEP's capability to detect the inflationary GWB with that of WMAP and Planck is demonstrated in Hivon & Kamionkowski [57]. They show that BICEP will achieve higher sensitivity to the GWB than these spaceborne experiments. BICEP's sensitivity results from advances in detector technology and from the ability to target only the cleanest regions of the microwave sky, rather than spreading out limited integration time over the full sky.

1.6.1 Optics

As outlined above, only modest angular resolution is required to detect the GWB's polarization signature. BICEP was designed to map $\sim 3\%$ of the sky with $0.9°$ resolution (at 100 GHz), $0.7°$ resolution (at 150 GHz), and $0.5°$ resolution (at 220 GHz). Unlike Planck or WMAP, BICEP was designed specifically for CMB polarimetry, able to modulate the polarization signal independent from the temperature signal with high fidelity. BICEP achieves this fidelity by virtue of an elegant optical design: a 4 kelvin refractor (Figure 1.5). Millimeter-wave radiation enters the instrument through a 30 cm diameter vacuum window and passes through heat-blocking filters cooled
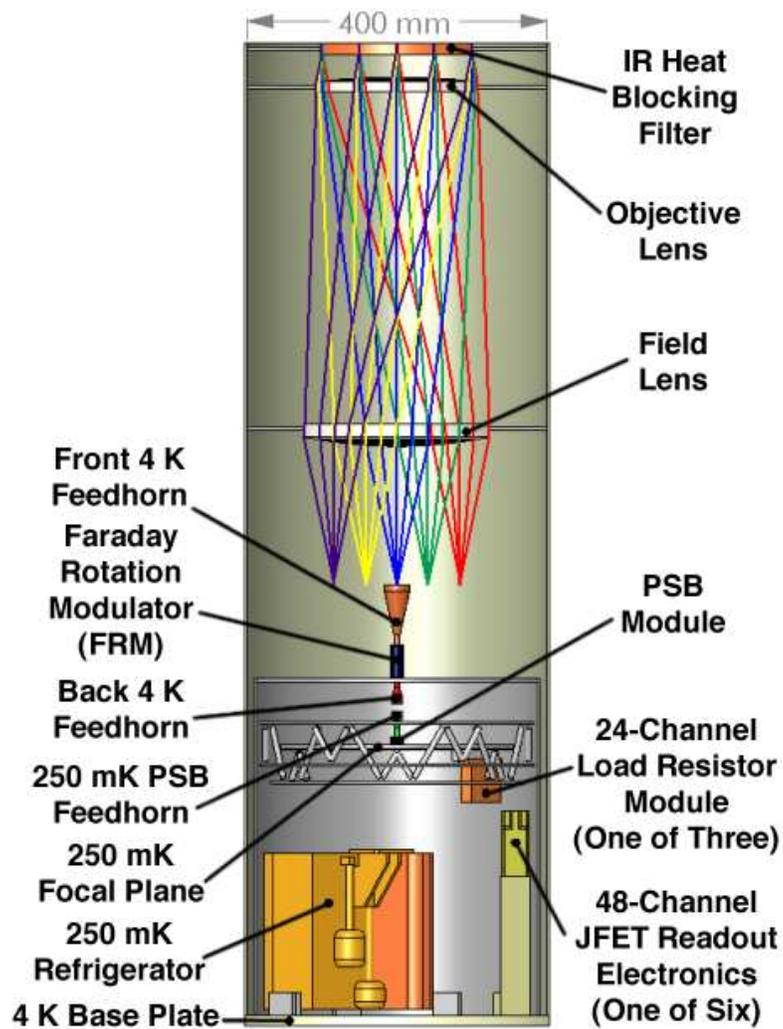
Fig. 1.5. A cross-sectional view of the BICEP receiver, which comprises a refracting telescope and 49 polarization-sensitive bolometers. The optics and focal plane are housed within a cryostat, which is placed on a three-axis mount. Figure credit: Thomas Renbarger.

to 4 K by liquid helium. Cold refractive optics produce diffraction-limited resolution over the entire 18° field-of-view.

1.6.2 Detector system

Each one of BICEP's 49 pixels comprises a complete polarimeter (optics, polarization modulator, analyzer, and detector). Each pixel uses three corrugated feedhorns feeding a polarization-sensitive bolometer pair (PSB), which simultaneously analyzes and detects linearly polarized light. The PSB's ingenious design is further described in [58]. In addition to their use in BICEP, PSBs have been successfully used in the *BOOMERANG* [59] and *QUAD* experiments to measure the E-mode polarization signal, and they will be used on Planck.

BICEP's PSBs use two absorbing grids, each coupled to a single linear polarization state. The (temperature-dependent) resistance of a semiconducting thermistor (neutron transmutation doped germanium; *NTD-Ge*), located at the edge of the absorber, detects CMB photons via a resistance change. BICEP's PSBs have astounding sensitivity: in one second, each PSB can detect temperature fluctuations as small as $\approx 450~\mu$K.

1.6.3 Polarization modulation

The faintness of the GWB polarization signal demands exquisite control of instrumental offsets. There are two ways to mitigate offsets: (1) minimize the offset and (2) modulate the signal before detection (Dicke switch) faster than the offset fluctuates. BICEP does both. A bridge-circuit differences the two PSBs within a single feed, producing a (first) difference signal that is null for an unpolarized input. This minimizes the offset. For six of the 49 spatial pixels, the polarized signal input is rapidly modulated (second difference) by Faraday Rotation Modulators (FRM) that rotate the plane of linear polarization of the incoming radiation. The FRMs make use of the Faraday Effect in a magnetized dielectric. Polarization modulation allows the polarized component of the CMB to be varied *independently* of the temperature signal, allowing the response of the telescope to remain fixed with respect to the (cold) sky and (warm) ground. This two-level differencing scheme allows for two levels of phase-sensitive detection, allowing optical systematic effects, associated with the telescope's antenna response pattern (leaking the much-larger CMB temperature signal to spurious CMB polarization), to be distinguished from true CMB polarization.

The FRMs represent a significant advance in the technology of CMB polarization modulation. Early CMB polarimeters (including Penzias and Wilson's, which *was* polarization-sensitive) used rotation of the entire telescope to modulate CMB polarization. These experiments [35, 36, 60] rotated hundreds or thousands of kilograms, were susceptible to vibration induced mi-

crophonic noise, and were limited mechanically to modulation rates < 0.1 Hz.

The next polarization modulation innovation was a birefringent half-waveplate: a single crystal of anisotropic dielectric (typically quartz or sapphire) that phase-delays one of the two linear polarizations [34, 61, 62]. While the fragile ~ 1 kg, cryogenically-cooled crystal *can* be rotated at ~ 1 Hz with lower-vibration than rotation of the entire telescope, such a mechanism is prone to failure since bearing operation is a severe challenge at cryogenic temperatures. And since bolometers are sensitive to power dissipation at the 10^{-17}W level, even minute mechanical vibrations produced by the bearings are intolerable.

Faraday Rotation Modulators†, shown in Figure 1.6, require only "rotating" electrons (the generation of a solenoidal magnetic field in a magnetized dielectric) to effect polarization rotation. Therefore, FRMs reduce the rotating mass that provides modulation by 30 orders of magnitude! Furthermore, these devices are capable of rotating polarized millimeter wave radiation at rates up to 10 kHz—faster than any conceivable time-varying temperature- or electronic-gain fluctuation. A superconducting NbTi solenoid wound around the waveguide provides the magnetic field that drives the ferrite into saturation, alternately parallel and anti-parallel to the propagation direction of the incoming radiation. The FRM rotates the CMB polarization vectors by $\pm 45°$ at 1 Hz, well above 1/f-fluctuation timescales (caused by, for example, temperature variations). The bolometer signals from the PSBs are detected using lock-in amplification.

1.6.4 Observations of galactic polarization using Faraday Rotation Modulators

Initial observations of the galactic plane were obtained during the austral winter of 2006. Several hundred hours of data were taken with the FRMs biased with a 1 Hz square wave. This modulation waveform effected $\pm 45°$ of polarization angle rotation. Other modulation waveforms can provide more or less rotation, as desired.

To validate the FRM technology we targeted several bright regions of the galactic plane. Results from some of these observations are displayed in Figure 1.7, where we also show the same region as imaged by WMAP [18]. The agreement is impressive. Because BICEP's bolometers simultaneously mea-

---

† US Patents Pending: "Wide Bandwidth Polarization Modulator, Switch, and Variable Attenuator," US Patent and Trademark Office, Serial Number: 60/689,740 (2005).
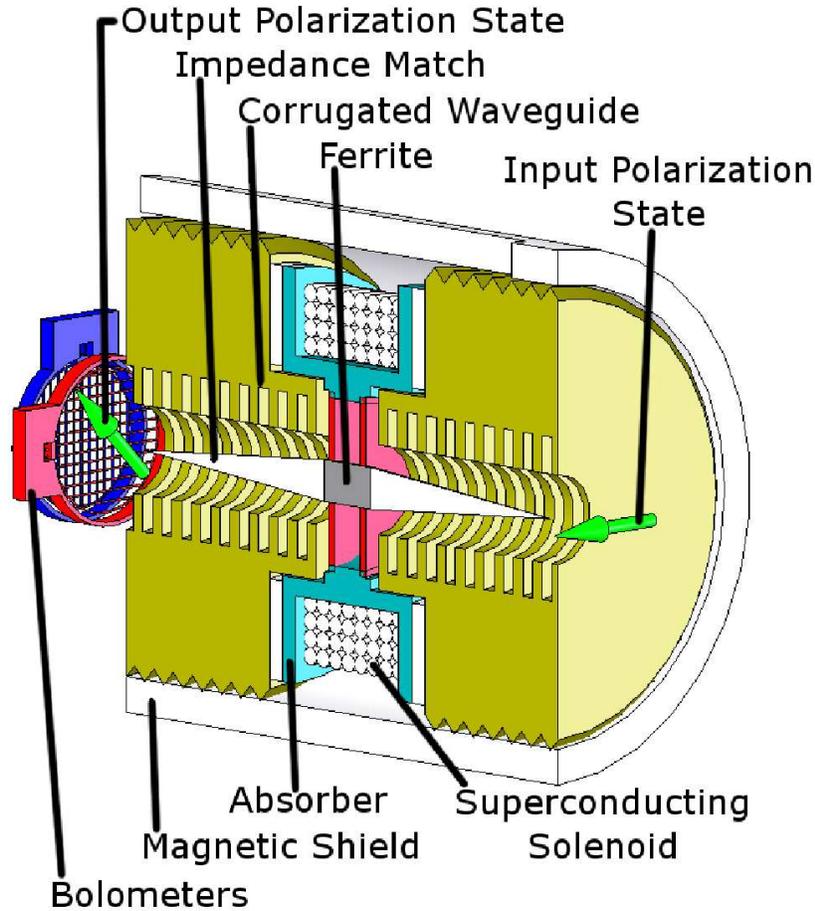
Fig. 1.6. A cross-sectional view of a Faraday Rotation Modulator (FRM) pixel. Polarized light enters from the right, is rotated by $\pm 45°$ and then analyzed (decomposed into orthogonal polarization components, which are detected individually by the polarization-sensitive bolometers, or PSBs). For each of BICEP's pixels, the PSBs are contained within a corrugated feedhorn, cooled to 0.25 K, located approximately 20 cm from the FRM, which is placed in a corrugated waveguide at the interface between two corrugated feedhorns, placed back-to-back and cooled to 4 K. The (schematic) location of the PSBs in this figure serves to illustrate the coordinate system used as the polarization basis. Figure credit: Thomas Renbarger.

sure polarization and temperature anisotropy, we use WMAP's temperature maps as a calibration source for BICEP.
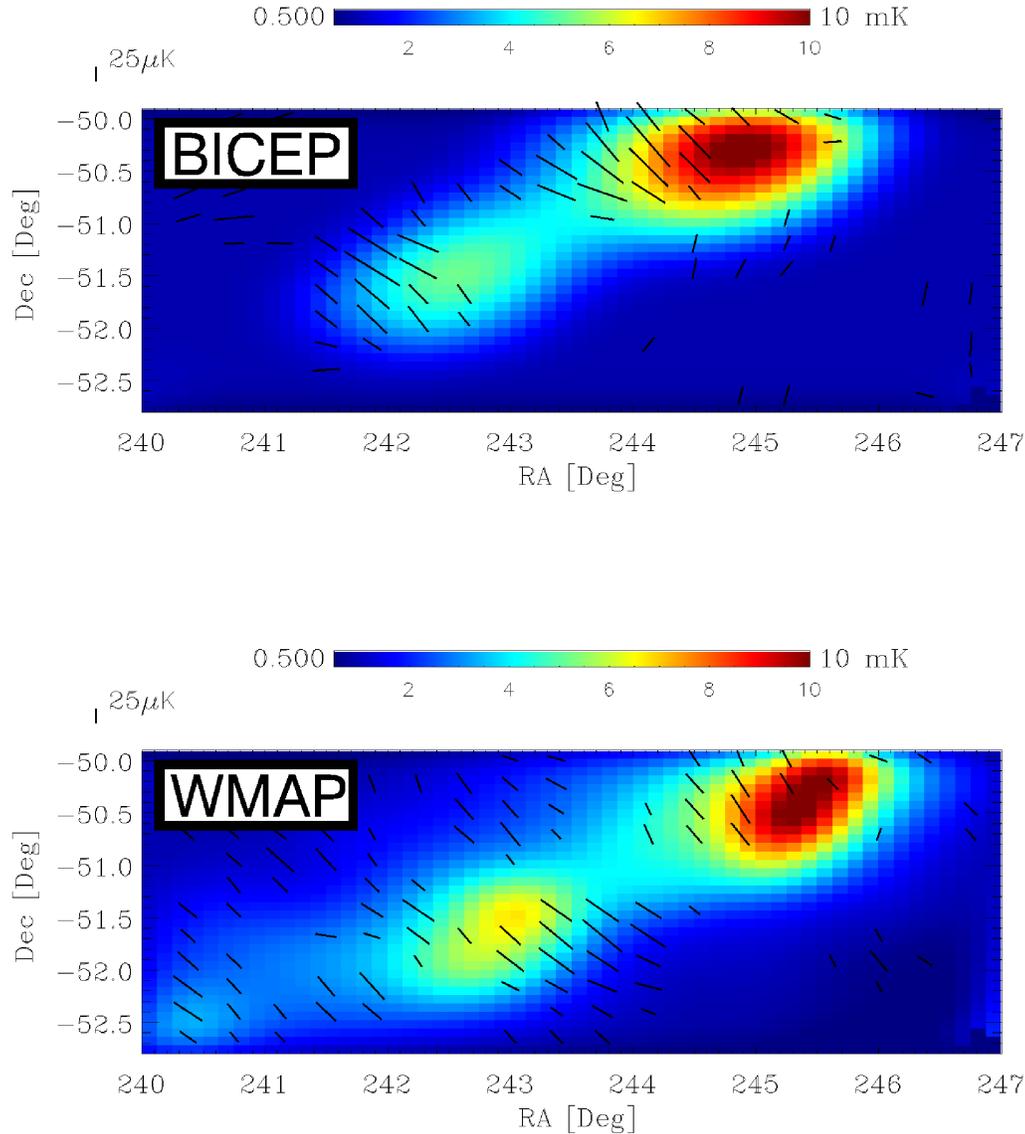
Fig. 1.7. Map of a portion of the galactic plane made using one of BICEP's six Faraday Rotation Modulator (FRM) pixels (top) operating at 100 GHz, compared to WMAP's observations of the same region (bottom). Microwave radiation is polarized by dust grains preferentially aligned by the galaxy's magnetic field. The FRM pixels modulate only the polarized component of the emission and can fully characterize linear polarization *without* rotation of the telescope. The short lines indicate the magnitude and orientation of the plane of polarization, and the gray scale indicates the temperature scale. For comparison, a scale bar representing 25 μK linear polarization is shown. The galactic plane extends approximately from the lower left to the upper right of each map. Both maps show significant linear polarization orthogonal to the galactic plane, which is expected as the galaxy's magnetic field is oriented parallel to the plane [18]. Similar maps were produced for BICEP's 150 GHz FRM pixels. We note that the BICEP FRM data were acquired over the course of a *week* of observations, whereas the WMAP data was obtained over three years. Figure credit: Evan Bierman.

1.6.5 The South Polar Observatory

Essential to achieving maximum sensitivity to CMB B-modes is the long integration time afforded by the South Pole site—arguably the premiere, long-duration, low-background (both natural and manmade) Earth-based site. To exploit this location, BICEP is highly efficient, having been designed for robustness and quasi-autonomous operation, while consuming a minimum of liquid cryogens (a precious commodity at the South Pole). BICEP's toroidal cryogen tanks house the instrument in a thermally uniform 4 K environment. The 49 polarimeter pixels, optics, and sub-Kelvin refrigerator are removable for easy instrument servicing. In December 2005, BICEP was installed at the US Amundsen-Scott South Pole Station's Dark Sector Laboratory, operated by the National Science Foundation. The Dark Sector Laboratory will house BICEP for three austral winter observing seasons and then house a future upgraded version, called BICEP-II, maximally leveraging the polar infrastructure investment for years to come.

More detail about the design of BICEP can be found in Keating *et al.* [53]. Preliminary data, maps, and additional technical information from BICEP's first observing season can be found in Yoon *et al.* [54].

1.7 Future probes of the past: BICEP-II, an advanced CMB polarimeter array

Following BICEP's initial phase, we will deploy an advanced high-density array to our South Pole observatory, eventually yielding ten-times better sensitivity than the first phase of BICEP. The GUT-scale is already nearly within the reach of current experiments [63], such as BICEP, and nearly all detectable inflationary models will ultimately be testable with BICEP-II's technology.

BICEP's NTD-Ge semiconducting detectors are background-limited, meaning the sensor's intrinsic noise is sub-dominant compared to the photon noise from atmospheric emission. In this regime, increasing the signal-to-noise ratio of the experiment can be accomplished only by adding detectors. After BICEP's three-year campaign concludes, our team will increase the number of detectors in BICEP's focal plane by a factor of more than five. This will produce a CCD-array-like focal plane which we call "BICEP-II."

BICEP-II will use the same optical design, observatory, and observing strategy as BICEP, but will be upgraded to an advanced detector-array of superconducting transition-edge sensors (TES). The TES [64] replaces the NTD-Ge semiconductor thermistor bonded to each absorbing grid in the current PSB design with a superconductor operated near its normal-to-

superconducting transition temperature. CMB photons heat up the super-conductor, causing its resistance to change enormously, which makes it an ideal sensor.

BICEP requires three electroformed feedhorn antennas per pixel both to receive power from the sky and to couple millimeter wave radiation to the bolometers, see Figure 1.5. The electroforming process is costly and time-consuming, and the feedhorn's dimensions fundamentally limit the packing efficiency of the focal plane. The TES methodology has a significant logistical advantage: the superconductor and associated components are all fabricated photolithographically, resulting in robust, reproducible, mass-produced arrays that can subsequently "tile" BICEP-II's focal plane. The tiling with planar arrays is extremely efficient— more than five times as many TES detectors can be placed in the same focal plane area as BICEP's current NTD-Ge semiconductor array.

BICEP-II will use TES bolometers with integrated planar antennae [65] developed at NASA/JPL and read-out by a time-domain SQUID multi-plexer developed at NIST [66]. The "ultimate" large angular scale B-mode experiment will be a small array of BICEP-II receivers at the South Pole. This array would use current technology to probe the GWB if inflation occurred at, or slightly below, the GUT-scale, thereby testing all potentially observable models of inflation. All of this can be accomplished *now* at the South Pole, for approximately 1% of the cost of a similarly capable satellite mission, allowing us to obtain perhaps the most enigmatic image ever captured: the birth pangs of the Big Bang!

References

[1] AH Guth. Inflationary universe: a possible solution to the horizon and flatness problems. *Phys Rev D*, **23** (1981 Jan), 347–56.

[2] J Khoury, BA Ovrut, PJ Steinhardt, and N Turok. Ekpyrotic universe: colliding branes and the origin of the hot big bang. *Phys Rev D*, **64** (12)(2001 Dec), 123522–+.

[3] J Magueijo. *Faster than the speed of light: the story of a scientific speculation.* Perseus Books, 2003.

[4] MS Turner. The new cosmology: mid-term report card for inflation. *Annales Henri Poincare*, **4** (2003), S333–S346.

[5] M Kamionkowski and A Kosowsky. Detectability of inflationary gravitational waves with microwave background polarization. *Phys Rev D*, **57** (1998 Jan), 685–91.

[6] Committee on the Physics of the Universe. *Connecting quarks with the cosmos: eleven science questions for the new century.* National Academies Press, 2003.

[7] *Astronomy and Astrophysics in the New Millennium.* National Academy Press, 2001.

[8] National Academies of Science Committee to Assess Progress Toward the Decadal Vision in Astronomy and Astrophysics. CM Urry, chair. The "Mid-Course Review" of the Astronomy and Astrophysics Decadal Survey.

[9] DOE/NSF High Energy Physics Advisory Panel Quantum Universe Committee. P Drell, chair. *Quantum Universe: The Revolution in 21st Century Particle Physics.*

[10] G Boerner. *The early universe: facts and fiction.* Springer, 2003.

[11] WH Kinney. Hamilton-Jacobi approach to non-slow-roll inflation. *Phys Rev D*, **56** (1997 Aug), 2002–9.

[12] M Kamionkowski and A Kosowsky. The cosmic microwave background and particle physics. *Annual Reviews of Nuclear and Particle Science*, **49** (1999), 77.

[13] http://lhc.web.cern.ch/lhc/.

[14] AR Liddle and DH Lyth. *Cosmological inflation and large-scale structure.* 2000.

[15] DN Spergel, R Bean, O Doré, MR Nolta, CL Bennett, J Dunkley, G Hinshaw, N Jarosik, E Komatsu, L Page, HV Peiris, L Verde, M Halpern, RS Hill, A Kogut, M Limon, SS Meyer, N Odegard, GS Tucker, JL Weiland, E Wollack, and EL Wright. Wilkinson Microwave Anisotropy Probe (WMAP) three year results: implications for cosmology. *ArXiv Astrophysics e-prints*, 2006 Mar.

[16] D Overbye. Scientists get glimpse of first moments after beginning of time. *New York Times*, 2006 Mar 16.

[17] DN Spergel and M Zaldarriaga. Cosmic microwave background polarization as a

direct test of inflation. *Physical Review Letters*, **79** (1997 Sep), 2180–3.

[18] L Page, G Hinshaw, E Komatsu, MR Nolta, DN.Spergel, CL Bennett, C Barnes, R Bean, O Doré, J Dunkley, M Halpern, RS Hill, N Jarosik, A Kogut, M Limon, SS Meyer, N Odegard, HV Peiris, GS Tucker, L Verde, JL Weiland, E Wollack, and EL Wright. Three year Wilkinson Microwave Anisotropy Probe (WMAP) observations: polarization analysis. *ArXiv Astrophysics e-prints*, 2006 Mar.

[19] AG Polnarev. Polarization and anisotropy induced in the microwave background by cosmological gravitational waves. *Soviet Astronomy*, **29** (1985 Dec), 607–+.

[20] P de Bernardis, PAR Ade, JJ Bock, JR Bond, J Borrill, A Boscaleri, K Coble, BP Crill, G De Gasperis, PC Farese, PG Ferreira, K Ganga, M Giacometti, E Hivon, VV Hristov, A Iacoangeli, AH Jaffe, AE Lange, L Martinis, S Masi, PV Mason, PD Mauskopf, A Melchiorri, L Miglio, T Montroy, CB Netterfield, E Pascale, F Piacentini, D Pogosyan, S Prunet, S Rao, G Romeo, JE Ruhl, F Scaramuzzi, D Sforna, and N Vittorio. A flat universe from high-resolution maps of the cosmic microwave background radiation. *Nature*, **404** (2000 Apr), 955–9.

[21] A Balbi, P Ade, J Bock, J Borrill, A Boscaleri, P De Bernardis, PG Ferreira, S Hanany, V Hristov, AH Jaffe, AT Lee, S Oh, E Pascale, B Rabii, PL Richards, GF Smoot, R Stompor, CD Winant, and JHP Wu. Constraints on cosmological parameters from MAXIMA-1. *Astrophys J Lett*, **545** (2000 Dec), L1–L4.

[22] C Pryke, NW Halverson, EM Leitch, J Kovac, JE Carlstrom, WL Holzapfel, and M Dragovan. Cosmological parameter extraction from the first season of observations with the degree angular scale interferometer. *Astrophys J*, **568** (2002 Mar), 46–51.

[23] JL Sievers, JR Bond, JK Cartwright, CR Contaldi, BS Mason, ST Myers, S Padin, TJ Pearson, U-L Pen, D Pogosyan, S Prunet, ACS Readhead, MC Shepherd, PS Udomprasert, L Bronfman, WL Holzapfel, and J May. Cosmological parameters from cosmic background imager observations and comparisons with BOOMERANG, DASI, and MAXIMA. *Astrophys J*, **591** (2003 Jul), 599–622.

[24] DN Spergel, L Verde, HV Peiris, E Komatsu, MR Nolta, CL Bennett, M Halpern, G Hinshaw, N Jarosik, A Kogut, M Limon, SS Meyer, L Page, GS Tucker, JL Weiland, E Wollack, and EL Wright. First-year Wilkinson Microwave Anisotropy Probe (WMAP) observations: determination of cosmological parameters. *Astrophysical Journal Supplement Series*, **148** (2003 Sep), 175–94.

[25] JH Goldstein, PAR Ade, JJ Bock, JR Bond, C Cantalupo, CR Contaldi, MD Daub, WL Holzapfel, C Kuo, AE Lange, M Lueker, M Newcomb, JB Peterson, D Pogosyan, JE Ruhl, MC Runyan, and E Torbet. Estimates of cosmological parameters using the cosmic microwave background angular power spectrum of ACBAR. *Astrophys J*, **599** (2003 Dec), 773–85.

[26] RH Dicke and PJ Peebles. Gravitation and space science. *Space Science Reviews*, **4** (1965), 419–+.

[27] ER Harrison. Fluctuations at the threshold of classical cosmology. *Phys Rev D*, **1** (1970), 2726.

[28] PJE Peebles and JT Yu. Primeval adiabatic perturbation in an expanding universe. *Astrophys J*, **162** (1970 Dec), 815–+.

[29] YB Zeldovich. A hypothesis, unifying the structure and the entropy of the universe. *MNRAS*, **160** (1972), 1P–+.

[30] DJ Eisenstein, I Zehavi, DW Hogg, R Scoccimarro, MR Blanton, RC Nichol, R Scranton, H Seo, M Tegmark, Z Zheng, S Anderson, J Annis, N Bahcall, J Brinkmann, S Burles, FJ Castander, A Connolly, I Csabai, M Doi, M Fukugita, JA Frieman, K Glazebrook, JE Gunn, JS Hendry, G Hennessy, Z Ivezic, S Kent,

GR Knapp, H Lin, Y Loh, RH Lupton, B Margon, T McKay, A Meiksin, JA Munn, A Pope, M Richmond, D Schlegel, D Schneider, K Shimasaku, C Stoughton, M Strauss, M Subbarao, AS Szalay, I Szapudi, D Tucker, B Yanny, and D York. Detection of the baryon acoustic peak in the large-scale correlation function of sdss luminous red galaxies. *submitted to ApJ, astro-ph/0501171*, (2005).

[31] S Cole, WJ Percival, JA Peacock, P Norberg, CM Baugh, CS Frenk, I Baldry, J Bland-Hawthorn, T Bridges, R Cannon, M Colless, C Collins, W Couch, NJG Cross, G Dalton, VR Eke, R De Propris, SP Driver, G Efstathiou, RS Ellis, K Glazebrook, C Jackson, A Jenkins, O Lahav, I Lewis, S Lumsden, S Maddox, D Madgwick, BA Peterson, W Sutherland, and K Taylor. The 2dF Galaxy Redshift Survey: power-spectrum analysis of the final data set and cosmological implications. *MNRAS*, **362** (2005 Sep), 505–34.

[32] MJ Rees. Polarization and spectrum of the primeval radiation in an anisotropic universe. *Astrophys J Lett*, 153 (1968 Jul), L1+.

[33] MM Basko and AG Polnarev. Polarization and anisotropy of the primordial radiation in an anisotropic universe. *Soviet Astronomy*, **57** (1980 May), 268.

[34] N Caderni, R Fabbri, B Melchiorri, F Melchiorri, and V Natale. Polarization of the microwave background radiation. II. an infrared survey of the sky. *Phys Rev D*, **17** (1978 Apr), 1908–18.

[35] PM Lubin and GF Smoot. Polarization of the cosmic background radiation. *Bulletin of the American Astronomical Society*, **11** (1979 Jun), 653–+.

[36] GP Nanos. Polarization of the blackbody radiation at 3.2 centimeters. *Astrophys J*, **232** (1979 Sep), 341–37.

[37] JM Kovac, EM Leitch, C Pryke, JE Carlstrom, NW Halverson, and WL Holzapfel. Detection of polarization in the cosmic microwave background using DASI. *Nature*, **420** (2002 Dec), 772–87.

[38] W Hu and M White. A CMB polarization primer. *New Astronomy*, **2** (1997 Oct), 323–44.

[39] M Kamionkowski, A Kosowsky, and A Stebbins. Statistics of cosmic microwave background polarization. *Phys Rev D*, **55** (1997 Jun), 7368–88.

[40] U Seljak and M Zaldarriaga. Signature of gravity waves in the polarization of the microwave background. *Physical Review Letters*, **78** (1997 Mar), 2054–7.

[41] L Knox and MS Turner. Detectability of tensor perturbations through anisotropy of the cosmic background radiation. *Physical Review Letters*, **73** (1994 Dec), 3347–50.

[42] LP Grishchuk. Quantum effects in cosmology. *Classical and Quantum Gravity*, **10** (1993 Dec), 2449–77.

[43] L Kofman, A Linde, and AA Starobinsky. Reheating after inflation. *Physical Review Letters*, **73** (1994 Dec), 3195–8.

[44] S Dodelson. *Modern cosmology.* Modern cosmology / Scott Dodelson. Amsterdam (Netherlands): Academic Press. ISBN 0-12-219141-2, 2003, XIII + 440 p., 2003.

[45] D Baskaran, LP Grishchuk, and AG Polnarev. Imprints of relic gravitational waves in cosmic microwave background radiation. *Phys Rev D*, **74** (8) (2006 Oct), :083008–+.

[46] Polnarev AG. Personal communication (2006).

[47] S Chongchitnan and G Efstathiou. Prospects for direct detection of primordial gravitational waves. *Phys Rev D*, **73** (8) (2006 Apr), 083511–+.

[48] TL Smith, M Kamionkowski, and A Cooray. Direct detection of the inflationary gravitational-wave background. *Phys Rev D*, **73** (2) (2006 Jan), 023504–+.

[49] TL Smith, E Pierpaoli, and M Kamionkowski. New cosmic microwave background constraint to primordial gravitational waves. *Physical Review Letters*, **97** (2) (2006

Jul), 021301–+.

[50] AA Penzias and RW Wilson. A measurement of excess antenna temperature at 4080 Mc/s. *Astrophys J*, **142** (1965 Jul), 419–21.

[51] GF Smoot, CL Bennett, A Kogut, EL Wright, J Aymon, NW Boggess, ES Cheng, G de Amici, S Gulkis, MG Hauser, G Hinshaw, PD Jackson, M Janssen, E Kaita, T Kelsall, P Keegstra, C Lineweaver, K Loewenstein, P Lubin, J Mather, SS Meyer, SH Moseley, T Murdock, L Rokke, RF Silverberg, L Tenorio, R Weiss, and DT Wilkinson. Structure in the COBE differential microwave radiometer first-year maps. *Astrophys J Lett*, **396** (1992 Sep), L1–L5.

[52] AH Jaffe, M Kamionkowski, and L Wang. Polarization pursuers' guide. *Phys Rev D*, **61** (8) (2000 Apr), 083501–+.

[53] BG Keating, PAR Ade, JJ Bock, E Hivon, WL Holzapfel, AE Lange, H Nguyen, and KW Yoon. BICEP: a large angular scale CMB polarimeter. In *Polarimetry in Astronomy. Proceedings of the SPIE*, ed. S Fineschi, vol. 4843 (2003 Feb), 284-95.

[54] KW Yoon, PAR Ade, D Barkats, JO Battle, EM Bierman, JJ Bock, JA Brevik, HC Chiang, A Crites, CD Dowell, L Duband, GS Griffin, EF Hivon, WL Holzapfel, VV Hristov, BG Keating, JM Kovac, CL Kuo, AE Lange, EM Leitch, PV Mason, HT Nguyen, N Ponthieu, YD Takahashi, T Renbarger, LC Weintraub, and D Woolsey. The Robinson Gravitational Wave Background Telescope (BICEP): a bolometric large angular scale CMB polarimeter. In *Millimeter and Submillimeter Detectors and Instrumentation for Astronomy III. Proceedings of the SPIE*, eds. J Zmuidzinas, WS Holland, S Withington, WD Duncan, vol. 6275 (2006 Jul), 62751K.

[55] FR Bouchet, A Benoit, Ph Camus, FX Desert, M Piat, and N.Ponthieu. Charting the new frontier of the cosmic microwave background polarization (2005).

[56] TE Montroy, PAR Ade, R Bihary, JJ Bock, JR Bond, J Brevick, CR Contaldi, BP Crill, A Crites, O Doré, L Duband, SR Golwala, M Halpern, G Hilton, W Holmes, VV Hristov, K Irwin, WC Jones, CL Kuo, AE Lange, CJ MacTavish, P Mason, J Mulder, CB Netterfield, E Pascale, JE Ruhl, A Trangsrud, C Tucker, A Turner, and M Viero. SPIDER: a new balloon-borne experiment to measure CMB polarization on large angular scales. In *Ground-based and Airborne Telescopes. Proceedings of the SPIE*, ed. LM Stepp, vol. 6267 (2006), 62670R. Presented at the Society of Photo-Optical Instrumentation Engineers (SPIE) Conference, 2006 Jul.

[57] E Hivon and M Kamionkowski. Opening a new window to the early universe. *ArXiv Astrophysics e-prints* (2002 Nov).

[58] WC Jones, R Bhatia, JJ Bock, and AE Lange. A polarization sensitive bolometric receiver for observations of the cosmic microwave background. In *Millimeter and Submillimeter Detectors for Astronomy. Proceedings of the SPIE*, eds. TG Phillips and J Zmuidzinas, vol. 4855 (2003 Feb), 227-38.

[59] TE Montroy, PAR Ade, JJ Bock, JR Bond, J Borrill, A Boscaleri, P Cabella, CR Contaldi, BP Crill, P de Bernardis, G De Gasperis, A de Oliveira-Costa, G De Troia, G di Stefano, E Hivon, AH Jaffe, TS Kisner, WC Jones, AE Lange, S Masi, PD Mauskopf, CJ MacTavish, A Melchiorri, P Natoli, CB Netterfield, E Pascale, F Piacentini, D Pogosyan, G Polenta, S Prunet, S Ricciardi, G Romeo, JE Ruhl, P Santini, M Tegmark, M Veneziani, and N Vittorio. A measurement of the CMB EE spectrum from the 2003 flight of BOOMERANG. *Astrophys J*, **647** (2006 Aug), 813–22.

[60] BG Keating, CW O'Dell, JO Gundersen, L Piccirillo, NC Stebor, and PT Timbie. An instrument for investigating the large angular scale polarization of the cosmic microwave background. *Astrophys J Supplement*, **144** (2003 Jan), 1–20.

[61] BJ Philhour. Measurement of the polarization of the cosmic microwave background.

Ph.D. Thesis (2002 Aug).

[62] BR Johnson, ME Abroe, P Ade, J Bock, J Borrill, JS Collins, P Ferreira, S Hanany, AH Jaffe, T Jones, AT Lee, L Levinson, T Matsumura, B Rabii, T Renbarger, PL Richards, GF Smoot, R Stompor, HT Tran, and CD Winant. MAXIPOL: a balloon-borne experiment for measuring the polarization anisotropy of the cosmic microwave background radiation. *New Astronomy Review*, **47** (2003 Dec), 1067–75.

[63] BG Keating, AG Polnarev, NJ Miller, and D Baskaran. The polarization of the cosmic microwave background due to primordial gravitational waves. *International Journal of Modern Physics A*, **21** (2006), 2459–79.

[64] JJ Bock. The promise of bolometers for CMB polarimetry. In *Polarimetry in Astronomy. Proceedings of the SPIE*, ed. S Fineschi, vol. 4843 (2003 Feb), 314-23.

[65] CL Kuo, JJ Bock, G Chattopadthyay, A Goldin, S Golwala, W Holmes, K Irwin, M Kenyon, AE Lange, HG LeDuc, P Rossinot, A Vayonakis, G Wang, M Yun, and J Zmuidzinas. Antenna-coupled TES bolometers for CMB polarimetry. In *Millimeter and Submillimeter Detectors and Instrumentation for Astronomy III. Proceedings of the SPIE*, eds. J Zmuidzinas, WS Holland, S Withington, WD Duncan, vol. 6275 (2006), 62751M. Presented at the Society of Photo-Optical Instrumentation Engineers (SPIE) Conference, 2006 Jul.

[66] PAJ de Korte, J Beyer, S Deiker, GC Hilton, KD Irwin, M Macintosh, SW Nam, CD Reintsema, LR Vale, and ME Huber. Time-division superconducting quantum interference device multiplexer for transition-edge sensors. *Review of Scientific Instruments*, **74** (2003 Aug), 3807–15.